


Article

High-Efficiency Skutterudite Modules at a Low Temperature Gradient

Wenjie Li ^{1,*}, David Stokes ², Bed Poudel ¹, Udara Saparamadu ¹, Amin Nozariasbmarz ¹ , Han Byul Kang ³ and Shashank Priya ^{1,*}

¹ Department of Materials Science and Engineering, Pennsylvania State University, University Park, PA 16802, USA; bup346@psu.edu (B.P.); uzs20@psu.edu (U.S.); aln192@psu.edu (A.N.)

² Electronics and Applied Physics Division, RTI International, Research Triangle Park, NC 27709, USA; stokes@ieee.org

³ Center for Energy Harvesting Materials and Systems (CEHMS), Virginia Tech, Blacksburg, VA 24060, USA; hbkang@vt.edu

* Correspondence: wzl175@psu.edu (W.L.); sup103@psu.edu (S.P.)

Received: 25 September 2019; Accepted: 5 November 2019; Published: 11 November 2019



Abstract: Thermoelectric skutterudite materials have been widely investigated for their potential application in mid-temperature waste heat recovery that has not been efficiently utilized. A large amount of research has focused on developing materials with a high thermoelectric figure of merit (zT). However, the translation of material properties to device performance has limited success. Here, we demonstrate single-filling n-type $\text{Yb}_{0.25}\text{Fe}_{0.25}\text{Co}_{3.75}\text{Sb}_{12}$ and multi-filling $\text{La}_{0.7}\text{Ti}_{0.1}\text{Ga}_{0.1}\text{Fe}_{2.7}\text{Co}_{1.3}\text{Sb}_{12}$ skutterudites with a maximum zT of ~ 1.3 at 740 K and ~ 0.97 at 760 K. The peak zT of skutterudites usually occurs above 800 K, but, as shown here, the shift in peak zT to lower temperatures is beneficial for enhancing conversion efficiency at a lower hot-side temperature. In this work, we have demonstrated that the Fe-substitution significantly reduces the thermal conductivity of n-type skutterudite, closer to p-type skutterudite thermal conductivity, resulting in a module that is more compatible to operate at elevated temperatures. A uni-couple skutterudite module was fabricated using a molybdenum electrode and Ga–Sn liquid metal as the thermal interface material. A conversion efficiency of 7.27% at a low temperature gradient of 366 K was achieved, which is among the highest efficiencies reported in the literature at this temperature gradient. These results highlight that peak zT shift and optimized module design can improve conversion efficiency of thermoelectric modules at a low temperature gradient.

Keywords: thermoelectric; skutterudite; conversion efficiency; temperature gradient

1. Introduction

Solid-state thermoelectric (TE) power generation technology is commonly used for converting waste thermal energy into electricity by utilizing the Seebeck effect. It provides a promising solution for energy harvesting from automobile exhausts, solar heat, waste heat from fuel cells, and industrial waste heat [1–3]. The conversion efficiency (η), given by Equation (1), is used to evaluate the TE performance,

$$\eta = \frac{T_h - T_c}{T_h} \cdot \frac{\sqrt{1 + zT_{ave}} - 1}{\sqrt{1 + zT_{ave}} + T_c/T_h} \quad (1)$$

where T_h is hot-side temperature and T_c is cold-side temperature. zT_{ave} is the average TE figure-of-merit determined by using the temperature range and materials zT , which is given by Equation (2),

$$zT = \frac{\alpha^2 \sigma}{\kappa} T \quad (2)$$

where α , σ , κ and T are the Seebeck coefficient, electrical conductivity, thermal conductivity and absolute temperature, respectively. Therefore, a high zT_{ave} is desirable, which can be obtained by either improving zT or by shifting peak zT to lower temperatures.

Among the state-of-the-art TE materials, CoSb₃-based skutterudites (SKD) have attracted much attention due to their comprehensive advantages, such as suitable band structure, electrical transport, low cost, and non-toxic constituent elements [4–9]. However, the large thermal conductivity of CoSb₃ results in poor zT , which leads to very low TE conversion efficiency. The large intrinsic nanocages that can be easily filled with various guest atoms promote SKD as an intriguing candidate for mid-temperature (473–773 K) waste heat recovery applications because of phonon glass-electron crystal behavior [10]. These fillers, such as alkali metals, alkaline-earth, rare-earth, and other ions [11] with a small ionic radius and heavy mass, can loosely bond to Sb atoms in nanocages and rattle in Einstein-like modes that function as a phonon-scattering source, resulting in low lattice thermal conductivity. Meanwhile, doping or substituting at the Co-site or Sb-site is another effective way to lower lattice thermal conductivity [11–14].

Yb-filled n-type skutterudites (n-SKD) show remarkable TE properties with maximum zT (zT_{max}) above 850 K [15–20], which is too high to maximize its performance for the mid-temperature region (473–773 K) under vacuum or 400–623 K in air [2,21]. In order to make it practical in real applications, it is essential to lower the zT_{max} temperature for enhancement of zT_{ave} . Single- and double-filling strategies have been utilized for improving zT of p-type skutterudites (p-SKD) [22–30]. The resonant frequencies of the fillers vary between 42 cm⁻¹ and 142 cm⁻¹ from rare-earth elements to alkali metals [31] so that phonons in different frequency ranges can be effectively scattered via phonon resonant scattering by the multi-fillers, which have been widely used for n-SKD [16,17,32]. However, the multi-filling p-SKD investigations are limited [33–35] and deserve further exploration. Moreover, for TE materials to result in device translation, mechanical stability is another critical consideration. The typical n-SKD with high zT usually has a relatively high thermal conductivity compared to p-SKD, which could lead to uneven thermal stress at elevated temperatures in TE modules and result in the mechanical failure of modules. Thus, the matching of thermal conductivity between n-SKD and p-SKD needs to be considered for long-term TE module performance. In this paper, our emphasis is on the development of compatible skutterudite materials and reduction of peak zT temperature to a lower temperature so that more stable and high-efficiency modules can be realized at temperatures below 700 K.

Developing higher zT materials has recently gained much interest in the thermoelectric community [16,19,33,36]. However, the transfer of excellent material properties to TE modules is lagging. Jesus et al. [37] and Park et al. [38] fabricated SKD modules focusing on high output power density. Salvador et al. [39] reported a maximum conversion efficiency (η_{max}) of 7% for a 32-couples SKD module at ΔT of 460 K with 4 mm height legs. Guo et al. and Geng et al. [24] have demonstrated 32-couples single-stage SKD modules with TE leg dimensions of 5 mm × 5 mm × 7.6 mm and achieved η_{max} of 8% at a temperature gradient (ΔT) of 550 K. Ge et al. [34] reported an improved η_{max} of 8.5% at ΔT of 550 K based on a 32-couples single stage SKD module with TE leg dimension of 5 mm × 5 mm × 7 mm. Zong et al. [40] developed a grain-boundary modified SKD that delivered an η_{max} of 8.4% under ΔT of 577 K. The module consisted of an 8-couples SKD with leg dimension of 4 mm × 4 mm × 12 mm. Ge and Li et al. [41] recently fabricated a 32-couples SKD module using bulk heterojunction-designed materials and demonstrated an η_{max} of 9.15% under ΔT of 600 K with leg dimensions of 5 mm × 5 mm × 7 mm. Zhang et al. [42] investigated a carbon-nanotube modified SKD and demonstrated an 8-couples module with an η_{max} of 9.3% under ΔT of 558 K. The TE leg dimensions in their design were 3 mm × 3 mm × 8 mm. However, in most of these studies, the ΔT was significantly high, at least >550 K, which requires a

hot-side temperature beyond 850 K and limits the application domain for SKD modules. Therefore, higher efficiency at lower ΔT is needed with hot-side temperature ~ 700 K to deploy SKD devices.

In this study, we demonstrate an n-type $\text{Yb}_{0.25}\text{Fe}_{0.25}\text{Co}_{3.75}\text{Sb}_{12}$ SKD with Fe-substitution on Co-site and a multi-filling $\text{La}_{0.7}\text{Ti}_{0.1}\text{Ga}_{0.1}\text{Fe}_{2.7}\text{Co}_{1.3}\text{Sb}_{12}$ p-type SKD with a nominal filling fraction of 0.9. The Yb-filler effectively reduces thermal conductivity due to its low rattling scattering frequency. The La/Ti/Ga-fillers cover a broad range of phonon scattering frequencies, leading to low thermal conductivity. The zT_{max} of ~ 1.3 for n-SKD was shifted to 740 K leading to an enhancement of zT_{ave} , and the zT_{max} of ~ 0.97 for p-SKD was obtained at 760 K. Through Fe-substitution, the total thermal conductivity of n-SKD was reduced to 2.5 W/m-K, which is comparable to that of p-SKD (~ 2 W/m-K). This results in a uniform heat transfer through n and p TE legs, which further increases the robustness of TE modules. A uni-couple TE module comprising of n-type $\text{Yb}_{0.25}\text{Fe}_{0.25}\text{Co}_{3.75}\text{Sb}_{12}$ and p-type $\text{La}_{0.7}\text{Ti}_{0.1}\text{Ga}_{0.1}\text{Fe}_{2.7}\text{Co}_{1.3}\text{Sb}_{12}$ was fabricated and tested. A molybdenum (Mo) electrode was bonded to the TE materials on the hot-side junction to provide good electrical and thermal contact. The Ga-Sn liquid metal was employed between the hot-side heat exchanger and the Mo electrode, as well as between the bottom ceramic substrate and a heat-sink used as a thermal interface material to reduce thermal resistance. Using this material combination, a high conversion efficiency of 7.27% is achieved under ΔT of 366 K, which is among the highest efficiencies reported at this temperature gradient.

2. Experimental Procedure

2.1. Materials Preparation

The skutterudite materials with $\text{Yb}_{0.25}\text{Fe}_{0.25}\text{Co}_{3.75}\text{Sb}_{12}$ composition for n-type and $\text{La}_{0.7}\text{Ti}_{0.1}\text{Ga}_{0.1}\text{Fe}_{2.7}\text{Co}_{1.3}\text{Sb}_{12}$ composition for p-type were prepared through a melting–quenching–annealing process. The high-purity elements Yb (99.9%, chips), La (99.9%, pieces), Ti (99.9%, wire), Ga (99.9%, pieces), Co (99.9%, pieces), Fe (99.99%, pieces) and Sb (99.9999%, shot) were weighed in an inert atmosphere according to their stoichiometric ratios, then loaded into graphite-coated quartz tubes and sealed under a vacuum. The sealed raw elements were slowly heated and melted at 1333 K for 20 h for n-type and 12 h for p-type, followed by quenching in NaCl saturated ice-water to obtain ingot. Then, the ingots were subsequently annealed at 973 K (n-type) and 923 K (p-type) for one week. Annealed materials were then hand-ground and sieved below 75 μm in the glovebox. Afterwards, the powders were pressed by Spark Plasma Sintering (SPS, SPS-615, FUJI ELECTRONIC INDUSTRIAL CO., LTD., Tsurugashima, Japan) at 923 K for n-type and 873 K for p-type under 40 MPa pressure for 5 min to achieve fully densified disks.

2.2. Materials Characterization

Powder X-ray diffraction (XRD) was performed using a Bruker D8 diffractometer with $\text{Cu-K}\alpha$ radiation ($\lambda = 1.5418 \text{ \AA}$) to check the phase purity. The Rietveld method was used to refine the structural parameters via the FullProf program for calculations. The microstructure was determined by scanning electron microscopy (SEM, FEI Quanta 600 FEG, Thermo Fisher Scientific, Hillsboro, USA), and actual compositions were detected via energy-dispersive X-ray spectroscopy (EDS). The density of specimens (ρ) was measured and calculated by the Archimedes method.

The electrical transport properties (electrical conductivity and Seebeck coefficient) were measured using the ZEM-3 system (ADVANCE-RIKO, Inc., Yokohama, Japan) up to 850 K. The thermal diffusivity (α) was measured by a laser flash system (ADVANCE-RIKO, Inc., TC-1200RH, Yokohama, Japan), and specific heat (C_p) was determined using a differential scanning calorimeter (NETZSCH GmbH, DSC 404C, Selb, Germany). Thermal conductivity, κ , was calculated from relation, $\kappa = \alpha\rho C_p$. The experimental uncertainties of electrical conductivity, thermal conductivity, Seebeck coefficient and zT are $\pm 5\%$, $\pm 2\%$, $\pm 5\%$ and $\pm 7\%$.

2.3. Module Fabrication and Test

The sintered n-type ($\text{Yb}_{0.25}\text{Fe}_{0.25}\text{Co}_{3.75}\text{Sb}_{12}$) and p-type ($\text{La}_{0.7}\text{Ti}_{0.1}\text{Ga}_{0.1}\text{Fe}_{2.7}\text{Co}_{1.3}\text{Sb}_{12}$) cylindrical pellets were diced into $1.8 \text{ mm} \times 1.8 \text{ mm} \times 2 \text{ mm}$ TE legs with a diamond dicing saw. The n- and p-type legs were then hard bonded with a molybdenum electrode on top, and a Cu electrode/AlN substrate on the bottom using a brazing process. The GaSn liquid metal was used between the bottom of the AlN substrate and the Q-meter, as well as between the heat exchanger and the Mo electrode as a thermal interface material. The uni-couple modules were prepared for power and efficiency tests. A custom-built power and efficiency testing system at RTI International was used to measure open voltage, current, internal resistance, output power and conversion efficiency of the modules. The heat flow was measured by a Q-meter using several thermal couples with specific distances. The hot-side temperature (T_h) was controlled from 310 K to 679 K, and the cold-side exchanger was cooled using circulating water. The uncertainties in output power and conversion efficiency are $\pm 3\%$ and $\pm 2\%$, respectively. A MATLAB program was used to calculate the theoretical conversion efficiency based on a method available in literature [43].

3. Results and Discussion

3.1. Materials Phase and Structure Analysis

The XRD patterns of densified pellets for both n-type $\text{Yb}_{0.25}\text{Fe}_{0.25}\text{Co}_{3.75}\text{Sb}_{12}$ and p-type $\text{La}_{0.7}\text{Ti}_{0.1}\text{Ga}_{0.1}\text{Fe}_{2.7}\text{Co}_{1.3}\text{Sb}_{12}$ show cubic $Im\bar{3}$ CoSb_3 phase, as shown in Figure 1 and Table 1. The Rietveld refinement shows a good fit with experimental observations. No impurity phase was detected, indicating that the total filler content is within the filling-fraction-limitation (FFL). The lattice parameters obtained from Rietveld refinement are 9.0511 \AA and 9.1173 \AA for n-SKD and p-SKD, respectively, which matches prior results available in the literature [15,16,20,27,44]. The lattice parameter of n-SKD increases with increasing Yb content. On the contrary, the lattice parameter of p-SKD decreases when the La content increases, and increases when Fe content increases, which is in agreement with our previous results [20].

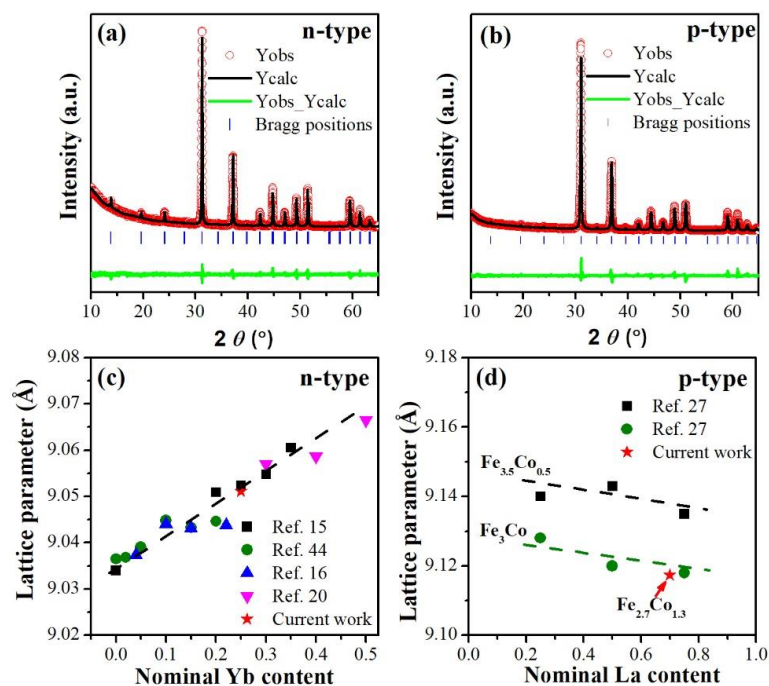
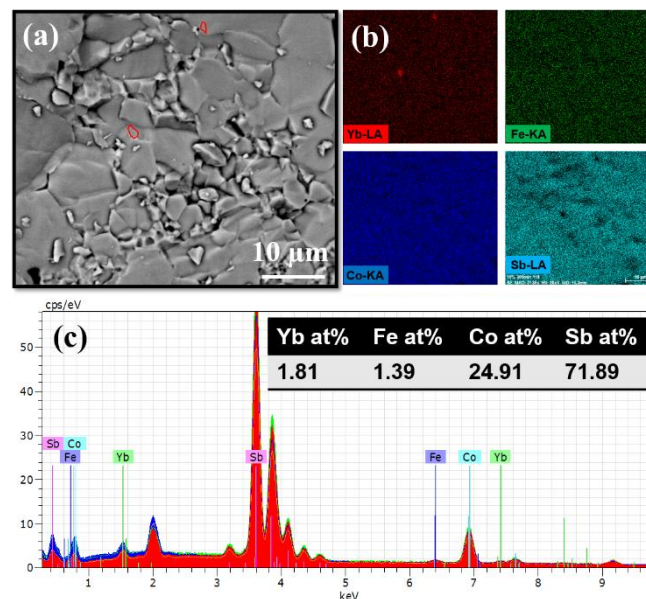


Figure 1. The Rietveld refinement of (a) n-type $\text{Yb}_{0.25}\text{Fe}_{0.25}\text{Co}_{3.75}\text{Sb}_{12}$ and (b) p-type $\text{La}_{0.7}\text{Ti}_{0.1}\text{Ga}_{0.1}\text{Fe}_{2.7}\text{Co}_{1.3}\text{Sb}_{12}$, and lattice parameters of (c) n-type $\text{Yb}_{0.25}\text{Fe}_{0.25}\text{Co}_{3.75}\text{Sb}_{12}$ and (d) p-type $\text{La}_{0.7}\text{Ti}_{0.1}\text{Ga}_{0.1}\text{Fe}_{2.7}\text{Co}_{1.3}\text{Sb}_{12}$. The comparison data are from References [15,16,20,27,44].

Table 1. Results of the Rietveld refinement analysis.

Samples	Lattice Parameters			R-Factors	
	a = b = c (Å)	Vol (Å ³)	Density (g/cm ³)	Rp (%)	Rwp (%)
n-Yb _{0.25} Fe _{0.25} Co _{3.75} Sb ₁₂	9.0511	741.487	7.567	3.55	3.53
p-La _{0.7} Ti _{0.1} Ga _{0.1} Fe _{2.7} Co _{1.3} Sb ₁₂	9.1173	757.869	7.866	4.69	3.28

The SEM images, EDS spectra and elemental distribution results for n-type Yb_{0.25}Fe_{0.25}Co_{3.75}Sb₁₂ and p-type La_{0.7}Ti_{0.1}Ga_{0.1}Fe_{2.7}Co_{1.3}Sb₁₂ are shown in Figures 2 and 3, respectively. For the n-type compound, the grain size is about 2–5 μm. The Yb filler distributes homogeneously in the matrix, besides some in situ YbSb₂ precipitates within a few hundred nanometers, which could effectively scatter phonons to reduce thermal conductivity, as shown in Figure 2a,b. The EDS analysis illustrates consistent atomic fraction of elements from different areas of the sample. This result is in agreement with stoichiometric atomic fraction, indicating no significant secondary phases or volatilization of Sb occurred during the synthesis process. For the p-type compound, various in situ precipitates were observed due to a high filling fraction, such as GaSb, TiSb₂ and LaTi, as shown in Figure 3a–c, with a variation of particle size from hundreds of nanometers to ~3 μm. Therefore, lower contents of La, Ti and Ga elements were detected compared to stoichiometric atomic fraction (Table 2). This is related to the fact that multi-filling compounds require faster cooling rates in order to obtain a more homogenous distribution of fillers compared to single-filling compounds [45]. Since all these precipitates were only in trace amounts (Figure 1a,b), the electrical properties would not be changed significantly, which will be discussed in Section 3.2.

**Figure 2.** (a) SEM image, (b) elemental distribution, and (c) EDS spectra of n-type Yb_{0.25}Fe_{0.25}Co_{3.75}Sb₁₂ compound.**Table 2.** Nominal and measured compositions, density (ρ), electrical conductivity (σ), Seebeck coefficient (α), and total thermal conductivity (κ_{total}) for n-type Yb_{0.25}Fe_{0.25}Co_{3.75}Sb₁₂ and p-type La_{0.7}Ti_{0.1}Ga_{0.1}Fe_{2.7}Co_{1.3}Sb₁₂ skutterudites at 298 K.

Nominal Composition	Measured Composition	ρ (g/cm ³)	σ (S/cm)	α (μ V/K)	κ_{total} (W/m·K)
Yb _{0.25} Fe _{0.25} Co _{3.75} Sb ₁₂	Yb _{0.29} Fe _{0.22} Co _{3.78} Sb _{11.68}	7.54	808	−178.25	2.34
La _{0.7} Ti _{0.1} Ga _{0.1} Fe _{2.7} Co _{1.3} Sb ₁₂	La _{0.54} Ti _{0.04} Ga _{0.05} Fe _{3.03} Co _{0.97} Sb _{11.4}	7.86	700	145.80	1.90

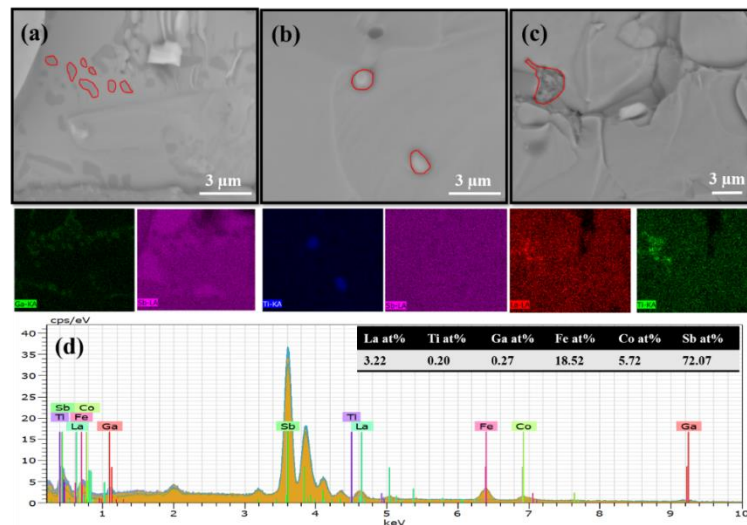


Figure 3. SEM image and elemental distribution of (a) GaSb precipitates, (b) TiSb₂ and (c) LaTi precipitates, and (d) EDS spectra of p-type La_{0.7}Ti_{0.1}Ga_{0.1}Fe_{2.7}Co_{1.3}Sb₁₂.

3.2. Material TE Properties

The TE properties at 298 K and bulk density (ρ) of n-type Yb_{0.25}Fe_{0.25}Co_{3.75}Sb₁₂ and p-type La_{0.7}Ti_{0.1}Ga_{0.1}Fe_{2.7}Co_{1.3}Sb₁₂ materials are summarized in Table 2. The measured composition for n-type skutterudite is consistent with the nominal one. The measured concentration of fillers in p-type skutterudite is lower compared to that of the nominal one due to the formation of various precipitates, as shown in Figure 3. The measured density is also consistent with the values calculated by refinement, as listed in Table 1. The material TE properties are shown in Figure 4. Since the substituted Fe in n-SKD is an electron acceptor, the electrical conductivity of n-SKD is relatively low, less than 900 S/cm and lower than that of CoSb₃-based n-SKD [15,19,46–48]. The electrical conductivity of p-SKD is about 700 S/cm and decreases with an increase in temperature. Both compounds exhibit metallic electrical conductivity behavior. The absolute Seebeck coefficients of n- and p-SKD increase with an increase in temperature and reach the maximum of 241.7 μ V/K at 740 K and 224.3 μ V/K at 760 K, respectively. Therefore, the maximum power factors of 36.2 μ W/cm \cdot K² for n-SKD and 25.8 μ W/cm \cdot K² for p-SKD materials were achieved below 800 K. Similarly, the total thermal conductivities of n-SKD and p-SKD decrease with an increase of temperature up to 600 K, and then increase due to the bipolar effect where both electron and holes carriers were excited and carried thermal energy at an elevated temperature. The lattice thermal conductivities are 1.2–2 W/m \cdot K for n-SKD and 1.1–1.7 W/m \cdot K for p-SKD materials, respectively. The n-SKD material shows very similar lattice thermal conductivity compared to that of p-SKD material at around 700 K due to the Fe-substitution. The carrier thermal conductivity shows a linear relationship with temperature, indicating that carriers can be thermally activated at elevated temperatures and contribute to both electrical and thermal conductivities, resulting in a bipolar effect. Moreover, a similar thermal conductivity between n-SKD and p-SKD can benefit uniform heat transfer through TE modules and release uneven thermal stress when heat flow increases at elevated temperatures. Overall, $zT_{max} \sim 1.3$ at 740 K was obtained for n-SKD material and ~ 0.97 at 760 K for p-SKD material. The zT_{max} shifted from above 800 K to around 750 K, as shown in Figure 4f. This will directly benefit the magnitude of the average zT and result in the enhancement of the conversion efficiency of a TE device.

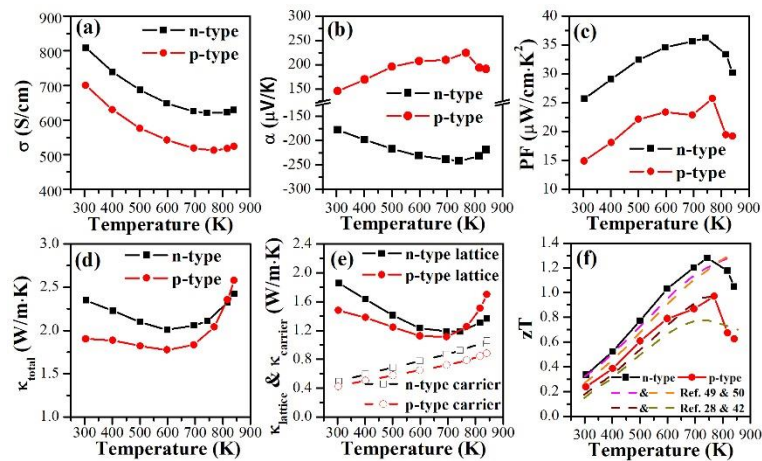


Figure 4. Summary of the thermoelectric (TE) properties. (a) electrical conductivity, (b) Seebeck coefficient, (c) power factor, (d) total thermal conductivity, (e) lattice and carrier thermal conductivity, and (f) zT for n-type $\text{Yb}_{0.25}\text{Fe}_{0.25}\text{Co}_{3.75}\text{Sb}_{12}$ and p-type $\text{La}_{0.7}\text{Ti}_{0.1}\text{Ga}_{0.1}\text{Fe}_{2.7}\text{Co}_{1.3}\text{Sb}_{12}$ materials. The dashed line data are from References [28,42,49,50].

3.3. Module Performance

The uni-couple SKD module was fabricated using n-type $\text{Yb}_{0.25}\text{Fe}_{0.25}\text{Co}_{3.75}\text{Sb}_{12}$ and p-type $\text{La}_{0.7}\text{Ti}_{0.1}\text{Ga}_{0.1}\text{Fe}_{2.7}\text{Co}_{1.3}\text{Sb}_{12}$ materials. In order to translate the materials zT to the conversion efficiency of a module, good electrical and thermal contact are critical factors. A Mo electrode was used because of its high thermal conductivity (~ 130 W/m·K) and low electrical resistivity ($\sim 5.2 \times 10^{-8}$ Ohm·m). The thermal stress and stability at high temperatures are important in order to maintain continuous module performance. The general thermal expansion coefficient (CTE) of SKD materials is about 8×10^{-6} /K for n-type and 10×10^{-6} /K for p-type [51]. The Mo electrode exhibits an excellent thermal stability and comparable CTE (5×10^{-6} /K) with that of SKD. The Ga–Sn liquid metal was used between the heat exchanger and the Mo electrode, as well as between AlN bottom substrate and Q-meter as a thermal interface material that reduces thermal resistance. The schematic configuration and picture of uni-couple SKD module is shown in Figure 5. The small TE leg dimensions of $1.8 \text{ mm} \times 1.8 \text{ mm} \times 2 \text{ mm}$ were used for the uni-couple module in order to reduce thermal stress and heat loss.

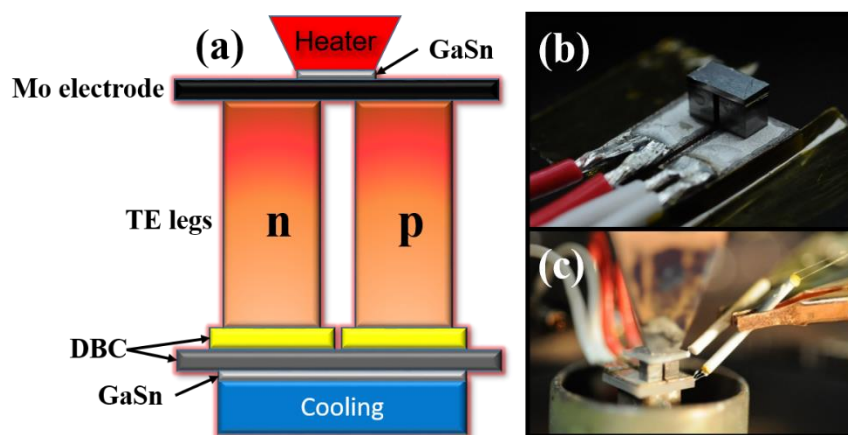


Figure 5. (a) The structure of skutterudites (SKD) uni-couple module, (b) the picture of SKD uni-couple module and (c) the SKD uni-couple module installed in the measurement system. The Direct Bond Copper (DBC) part includes Cu electrode (yellow parts) and AlN substrate (dark gray part).

The temperature-dependent module resistance, open-circuit voltage, output power, and conversion efficiency were measured under hot-side temperature up to 679 K, as shown in Figure 6. The internal

module resistance shows a linear relationship with ΔT , which aligns with the decrease of the electrical conductivity of materials at an elevated temperature. The linear increase of open-circuit voltage as ΔT rises from 38 K to 366 K is consistent with the increased absolute Seebeck coefficient. The maximum output power (P_{max}) of 336.7 mW is obtained with a ΔT of 366 K ($T_h = 679$ K, $T_c = 313$ K). The conversion efficiency is calculated using Equation (3),

$$\eta = \frac{P}{Q_{in}} = \frac{P}{P + Q_{out}} \times 100\% \tag{3}$$

where P is output power, Q_{in} is hot-side heat flow and Q_{out} is cold-site heat flow. A maximum conversion efficiency (η_{max}) of 7.27% is obtained with a hot-side temperature of 679 K and ΔT of 366 K. Ga-Sn is found to fully wet the interface between the heat exchanger and the Mo electrode/AlN ceramic substrate at an elevated temperature that minimizes thermal resistance and enhances heat transfer. The MATLAB-simulated theoretical conversion efficiency (dash line in Figure 6c) is based on the experimental TE properties of 8.69% at ΔT of 366 K. The difference between theoretical and experimental efficiency can be attributed to interfacial electrical and thermal resistance between the TE legs and the substrate, as well as the thermal radiation and convection losses [40]. The conversion efficiency obtained in this study (Figure 6d) provides a great advantage with smaller ΔT compared to previously reported efficiencies of single-stage SKD modules [24,34,35,40,42]. The consistent module resistance of 15.1 mOhm before test and 15.2 mOhm after test illustrates that the bonding process utilized here provides robust modules.

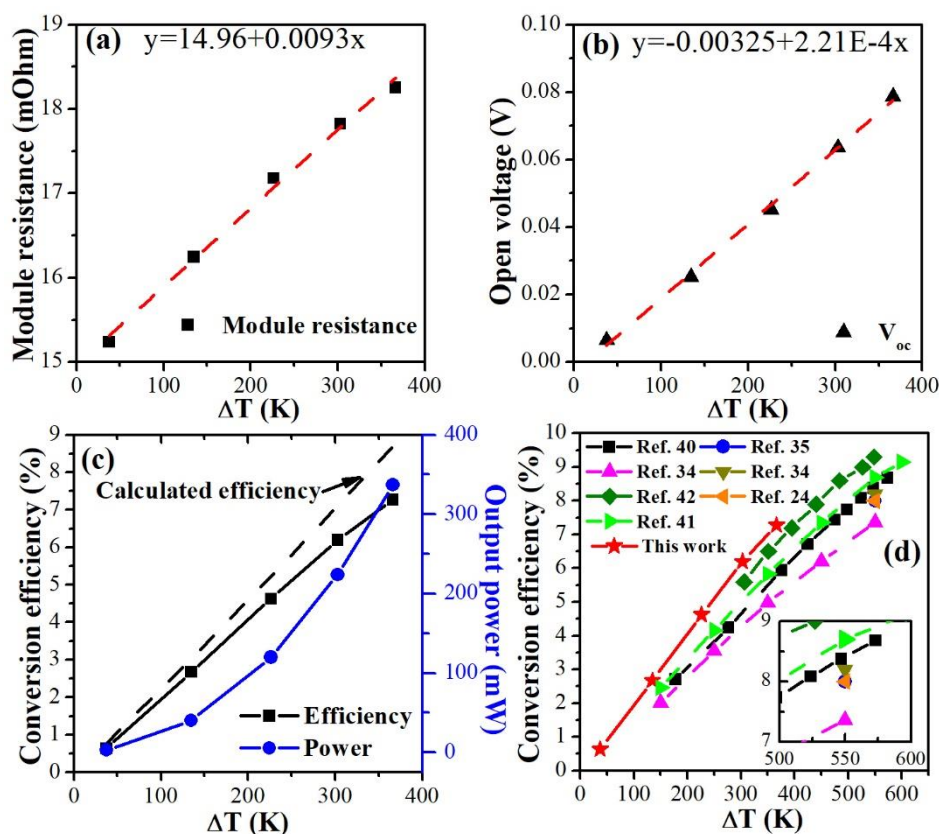


Figure 6. (a) The internal resistance, (b) open voltage, (c) conversion efficiency and output power of SKD module as a function of ΔT , and (d) the comparison of conversion efficiency between our result and the literature results (References [24,34,35,40–42]).

4. Conclusions

In this study, a single-filling n-type $\text{Yb}_{0.25}\text{Fe}_{0.25}\text{Co}_{3.75}\text{Sb}_{12}$ with Fe-substitution on Co-site and multi-filling p-type $\text{La}_{0.7}\text{Ti}_{0.1}\text{Ga}_{0.1}\text{Fe}_{2.7}\text{Co}_{1.3}\text{Sb}_{12}$ were synthesized via a melting–quenching–annealing process. The zT_{max} of ~ 1.3 was obtained at 740 K and ~ 0.97 at 760 K for n-type and p-type SKD material, respectively. By lowering zT_{max} temperatures, we have shown an enhancement of zT_{avg} resulting in an improvement in the thermoelectric conversion efficiency. The comparable thermal conductivity of n- and p-type SKD contributes to the development of a more thermally stable TE module due to the balance of heat flow from p and n materials. The fabricated uni-couple SKD from these materials demonstrates a high conversion efficiency of 7.27% under ΔT of only 366 K when the hot-side temperature is 679 K. This efficiency value is among the highest conversion efficiency reported for single-stage SKD modules at this temperature gradient. These results provide a promising pathway for using SKD materials for mid-temperature power generation applications, as well as for cascaded or segmented TE modules with half-Heusler materials to realize even higher conversion efficiencies. This work further demonstrates that the zT peak shifting is a promising technique of realizing high conversion efficiency in a desired operation temperature range.

Author Contributions: Conceptualization, W.L.; Data curation, W.L. and D.S.; Funding acquisition, S.P.; Investigation, W.L. and D.S.; Methodology, W.L.; Resources, S.P.; Software, W.L. and U.S.; Supervision, B.P. and S.P.; Writing—Original draft, W.L.; Writing—Review & editing, D.S., B.P., U.S., A.N., H.B.K. and S.P.

Funding: This research was funded by the office of Defense Advanced Research Projects Agency (DARPA) under the project of Nano Engineered Thermoelectric Systems (NETS).

Conflicts of Interest: The authors declare no conflict of interest.

References

1. Zebarjadi, M.; Esfarjani, K.; Dresselhaus, M.S.; Ren, Z.F.; Chen, G. Perspectives on thermoelectrics: From fundamentals to device applications. *Energy Environ. Sci.* **2012**, *5*, 5147–5162. [[CrossRef](#)]
2. Champier, D. Thermoelectric generators: A review of applications. *Energy Convers. Manag.* **2017**, *140*, 167–181. [[CrossRef](#)]
3. Fairbanks, J.W. Automotive Thermoelectric Generators and HVAC. In Proceedings of the Directions in Engine-Efficiency and Emissions Research Conference (DEER), Dearborn, MI, USA, 16–19 October 2012.
4. Sales, B.C.; Mandrus, D.; Williams, R.K. Filled skutterudite antimonides: A new class of thermoelectric materials. *Science* **1996**, *272*, 1325–1328. [[CrossRef](#)] [[PubMed](#)]
5. Nolas, G.S.; Morelli, D.T.; Tritt, T.M. Skutterudites: A phonon-glass-electron crystal approach to advanced thermoelectric energy conversion applications. *Annu. Rev. Mater. Sci.* **1999**, *29*, 89–116. [[CrossRef](#)]
6. Uher, C. Skutterudites: Prospective novel thermoelectrics. In *Semiconduct and Semimetals*; Elsevier: Amsterdam, The Netherlands, 2001; Volume 69, pp. 139–253.
7. Snyder, G.J.; Toberer, E.S. Complex thermoelectric materials. *Nat. Mater.* **2008**, *7*, 105–114. [[CrossRef](#)] [[PubMed](#)]
8. Luo, H.X.; Krizan, J.W.; Muechler, L.; Haldolaarachchige, N.; Klimczuk, T.; Xie, W.W.; Fucillo, M.K.; Felser, C.; Cava, R.J. A large family of filled skutterudites stabilized by electron count. *Nat. Commun.* **2015**, *6*. [[CrossRef](#)] [[PubMed](#)]
9. Rogl, G.; Rogl, P. Skutterudites, a most promising group of thermoelectric materials. *Curr. Opin. Green Sustain. Chem.* **2017**, *4*, 50–57. [[CrossRef](#)]
10. Slack, G.A. *CRC Handbook of Thermoelectrics*; CRC Press: Boca Raton, FL, USA, 1995.
11. Wan, S.; Huang, X.Y.; Qiu, P.F.; Shi, X.; Chen, L.D. Compound Defects and Thermoelectric Properties of Self-Charge Compensated Skutterudites $\text{SeyCo}_4\text{Sb}_{12-x}\text{Sex}$. *ACS Appl. Mater. Interfaces* **2017**, *9*, 22713–22724. [[CrossRef](#)] [[PubMed](#)]
12. Sun, H.R.; Jia, X.P.; Deng, L.; Lv, P.; Guo, X.; Zhang, Y.W.; Sun, B.; Liu, B.W.; Ma, H.G. Effect of HPHT processing on the structure, and thermoelectric properties of $\text{Co}_4\text{Sb}_{12}$ co-doped with Te and Sn. *J. Mater. Chem. A* **2015**, *3*, 4637–4641. [[CrossRef](#)]
13. Xu, C.L.; Duan, B.; Ding, S.J.; Zhai, P.C.; Li, P. Thermoelectric transport properties of nickel-doped $\text{Co}_{4-x}\text{Ni}_x\text{Sb}_{11.6}\text{Te}_{0.2}\text{Se}_{0.2}$ skutterudites. *Phys. B Condens. Matter* **2013**, *425*, 34–37. [[CrossRef](#)]

14. Wojciechowski, K.T.; Tobola, J.; Leszczynski, J. Thermoelectric properties and electronic structure of CoSb₃ doped with Se and Te. *J. Alloys Compd.* **2003**, *361*, 19–27. [[CrossRef](#)]
15. Wang, S.Y.; Salvador, J.R.; Yang, J.; Wei, P.; Duan, B.; Yang, J.H. High-performance n-type Yb_xCo₄Sb₁₂: From partially filled skutterudites towards composite thermoelectrics. *NPG Asia Mater.* **2016**, *8*, e285. [[CrossRef](#)]
16. Shi, X.; Yang, J.; Salvador, J.R.; Chi, M.F.; Cho, J.Y.; Wang, H.; Bai, S.Q.; Yang, J.H.; Zhang, W.Q.; Chen, L.D. Multiple-Filled Skutterudites: High Thermoelectric Figure of Merit through Separately Optimizing Electrical and Thermal Transports. *J. Am. Chem. Soc.* **2011**, *133*, 7837–7846. [[CrossRef](#)] [[PubMed](#)]
17. Rogl, G.; Grytsiv, A.; Rogl, P.; Peranio, N.; Bauer, E.; Zehetbauer, M.; Eibl, O. n-Type skutterudites (R,Ba,Yb)_yCo₄Sb₁₂ (R = Sr, La, Mm, DD, SrMm, SrDD) approaching ZT approximate to 2.0. *Acta Mater.* **2014**, *63*, 30–43. [[CrossRef](#)]
18. Hanus, R.; Guo, X.Y.; Tang, Y.L.; Li, G.D.; Snyder, G.J.; Zeier, W.G. A Chemical Understanding of the Band Convergence in Thermoelectric CoSb₃ Skutterudites: Influence of Electron Population, Local Thermal Expansion, and Bonding Interactions. *Chem. Mater.* **2017**, *29*, 1156–1164. [[CrossRef](#)]
19. Zong, P.A.; Chen, X.H.; Zhu, Y.W.; Liu, Z.W.; Zeng, Y.; Chen, L.D. Construction of a 3D-rGO network-wrapping architecture in a Yb_yCo₄Sb₁₂/rGO composite for enhancing the thermoelectric performance. *J. Mater. Chem. A* **2015**, *3*, 8643–8649. [[CrossRef](#)]
20. Li, W.; Wang, J.; Xie, Y.; Gray, J.L.; Heremans, J.J.; Kang, H.B.; Poudel, B.; Huxtable, S.T.; Priya, S. Enhanced Thermoelectric Performance of Yb-Single-Filled Skutterudite by Ultralow Thermal Conductivity. *Chem. Mater.* **2019**, *31*, 862–872. [[CrossRef](#)]
21. Fairbanks, J.W.V. Thermoelectrics: A New Green Technology in Directions in Engine-Efficiency and Emission Research. Detroit, Michigan. Available online: <https://www.energy.gov/eere/vehicles/2011-directions-engine-efficiency-and-emissions-research-deer-conference-presentations> (accessed on 9 November 2019).
22. Tang, X.F.; Li, H.; Zhang, Q.J.; Niino, M.; Goto, T. Synthesis and thermoelectric properties of double-atom-filled skutterudite compounds Ca_mCe_nFe_xCo_{4-x}Sb₁₂. *J. Appl. Phys.* **2006**, *100*. [[CrossRef](#)]
23. Tan, G.J.; Wang, S.Y.; Tang, X.F.; Li, H.; Uher, C. Preparation and thermoelectric properties of Ga-substituted p-type fully filled skutterudites CeFe_{4-x}Ga_xSb₁₂. *J. Solid State Chem.* **2012**, *196*, 203–208. [[CrossRef](#)]
24. Geng, H.Y.; Ochi, T.; Suzuki, S.; Kikuchi, M.; Ito, S.; Guo, J.Q. Thermoelectric Properties of Multifilled Skutterudites with La as the Main Filler. *J. Electron. Mater.* **2013**, *42*, 1999–2005. [[CrossRef](#)]
25. Lu, P.X.; Qu, L.B.; Cheng, Q.H. Enhancement of thermoelectric figure of merit in binary-phased La_{0.3}Ce_{0.37}Fe₃CoS₁₂-PbTe materials. *J. Alloys Compd.* **2013**, *558*, 50–55. [[CrossRef](#)]
26. Tan, G.J.; Zheng, Y.; Tang, X.F. High thermoelectric performance of nonequilibrium synthesized CeFe₄Sb₁₂ composite with multi-scaled nanostructures. *Appl. Phys. Lett.* **2013**, *103*. [[CrossRef](#)]
27. Joo, G.S.; Shin, D.K.; Kim, I.H. Thermoelectric Properties of Double-Filled p-Type La_{1-z}Yb_zFe_{4-x}Co_xSb₁₂ Skutterudites. *J. Electron. Mater.* **2015**, *44*, 1383–1387. [[CrossRef](#)]
28. Fu, L.W.; Jiang, Q.H.; Yang, J.Y.; Peng, J.Y.; Xiao, Y.; Luo, Y.B.; Zhou, Z.W.; Zhang, D. Enhancement of thermoelectric properties of Ce_{0.9}Fe_{3.75}Ni_{0.25}Sb₁₂ p-type skutterudite by tellurium addition. *J. Mater. Chem. A* **2016**, *4*, 16499–16506. [[CrossRef](#)]
29. Ortiz, B.R.; Crawford, C.M.; McKinney, R.W.; Parilla, P.A.; Toberer, E.S. Thermoelectric properties of bromine filled CoSb₃ skutterudite. *J. Mater. Chem. A* **2016**, *4*, 8444–8450. [[CrossRef](#)]
30. Kim, J.; Kurosaki, K.; Choi, S.; Ohishi, Y.; Muta, H.; Yamanaka, S.; Takahashi, M.; Tanaka, J. Thermoelectric Properties of In_xFeCo₃Sb₁₂ Consisting Mainly of In-Filled p-Type Skutterudites. *Mater. Trans.* **2017**, *58*, 1207–1211. [[CrossRef](#)]
31. Yang, J.; Zhang, W.; Bai, S.Q.; Mei, Z.; Chen, L.D. Dual-frequency resonant phonon scattering in Ba_xRyCo₄Sb₁₂ (R=La, Ce, and Sr). *Appl. Phys. Lett.* **2007**, *90*. [[CrossRef](#)]
32. Ballikaya, S.; Uzar, N.; Yildirim, S.; Salvador, J.R.; Uher, C. High thermoelectric performance of In, Yb, Ce multiple filled CoSb₃ based skutterudite compounds. *J. Solid State Chem.* **2012**, *193*, 31–35. [[CrossRef](#)]
33. Ren, W.; Geng, H.Y.; Zhang, L.X.; Liu, X.P.; He, T.H.; Feng, J.C. Simultaneous blocking of minority carrier and high energy phonon in p-type skutterudites. *Nano Energy* **2018**, *46*, 249–256. [[CrossRef](#)]
34. Nie, G.; Suzuki, S.; Tomida, T.; Sumiyoshi, A.; Ochi, T.; Mukaiyama, K.; Kikuchi, M.; Guo, J.Q.; Yamamoto, A.; Obara, H. Performance of Skutterudite-Based Modules. *J. Electron. Mater.* **2017**, *46*, 2640–2644. [[CrossRef](#)]
35. Guo, J.Q.; Geng, H.Y.; Ochi, T.; Suzuki, S.; Kikuchi, M.; Yamaguchi, Y.; Ito, S. Development of Skutterudite Thermoelectric Materials and Modules. *J. Electron. Mater.* **2012**, *41*, 1036–1042. [[CrossRef](#)]

36. Rogl, G.; Grytsiv, A.; Rogl, P.; Bauer, E.; Zehetbauer, M. A new generation of p-type didymium skutterudites with high ZT. *Intermetallics* **2011**, *19*, 546–555. [[CrossRef](#)]
37. Prado-Gonjal, J.; Phillips, M.; Vaqueiro, P.; Min, G.; Powell, A.V. Skutterudite Thermoelectric Modules with High Volume-Power Density: Scalability and Reproducibility. *ACS Appl. Energy Mater.* **2018**, *1*, 6609–6618. [[CrossRef](#)]
38. Park, S.H.; Jin, Y.; Cha, J.; Hong, K.; Kim, Y.; Yoon, H.; Yoo, C.Y.; Chung, I. High-Power-Density Skutterudite-Based Thermoelectric Modules with Ultralow Contact Resistivity Using Fe-Ni Metallization Layers. *ACS Appl. Energy Mater.* **2018**, *1*, 1603–1611. [[CrossRef](#)]
39. Salvador, J.R.; Cho, J.Y.; Ye, Z.X.; Moczygemba, J.E.; Thompson, A.J.; Sharp, J.W.; Koenig, J.D.; Maloney, R.; Thompson, T.; Sakamoto, J.; et al. Conversion efficiency of skutterudite-based thermoelectric modules. *Phys. Chem. Chem. Phys.* **2014**, *16*, 12510–12520. [[CrossRef](#)] [[PubMed](#)]
40. Zong, P.A.; Hanus, R.; Dylla, M.; Tang, Y.S.; Liao, J.C.; Zhang, Q.H.; Snyder, G.J.; Chen, L.D. Skutterudite with graphene-modified grain-boundary complexation enhances zT enabling high-efficiency thermoelectric device. *Energy Environ. Sci.* **2017**, *10*, 183–191. [[CrossRef](#)]
41. Nie, G.; Li, W.; Guo, J.; Yamamoto, A.; Kimura, K.; Zhang, X.; Isaacs, E.B.; Druvid, V.; Wolverton, C.; Kanatzidis, M.G.; et al. High performance thermoelectric module through isotope bulk heterojunction engineering of skutterudite materials. *Nano Energy* **2019**. [[CrossRef](#)]
42. Zhang, Q.H.; Zhou, Z.X.; Dylla, M.; Agne, M.T.; Pei, Y.Z.; Wang, L.J.; Tang, Y.S.; Liao, J.C.; Li, J.; Bai, S.Q.; et al. Realizing high-performance thermoelectric power generation through grain boundary engineering of skutterudite-based nanocomposites. *Nano Energy* **2017**, *41*, 501–510. [[CrossRef](#)]
43. Kim, H.S.; Liu, W.S.; Chen, G.; Chua, C.W.; Ren, Z.F. Relationship between thermoelectric figure of merit and energy conversion efficiency. *Proc. Natl. Acad. Sci. USA* **2015**, *112*, 8205–8210. [[CrossRef](#)] [[PubMed](#)]
44. Dilley, N.R.; Bauer, E.D.; Maple, M.B.; Sales, B.C. Thermoelectric properties of chemically substituted skutterudites $\text{Yb}_y\text{Co}_4\text{Sn}_x\text{Sb}_{12-x}$. *J. Appl. Phys.* **2000**, *88*, 1948–1951. [[CrossRef](#)]
45. Tan, G.J.; Liu, W.; Wang, S.Y.; Yan, Y.G.; Li, H.; Tang, X.F.; Uher, C. Rapid preparation of $\text{CeFe}_4\text{Sb}_{12}$ skutterudite by melt spinning: Rich nanostructures and high thermoelectric performance. *J. Mater. Chem. A* **2013**, *1*, 12657–12668. [[CrossRef](#)]
46. Fu, L.W.; Yang, J.Y.; Peng, J.Y.; Jiang, Q.H.; Xiao, Y.; Luo, Y.B.; Zhang, D.; Zhou, Z.W.; Zhang, M.Y.; Cheng, Y.D.; et al. Enhancement of thermoelectric properties of Yb-filled skutterudites by an Ni-Induced “core-shell” structure. *J. Mater. Chem. A* **2015**, *3*, 1010–1016. [[CrossRef](#)]
47. Li, Y.L.; Qiu, P.F.; Duan, H.Z.; Chen, J.K.; Snyder, G.J.; Shi, X.; Iversen, B.B.; Chen, L.D. Enhanced thermoelectric performance in rare-earth filled-skutterudites. *J. Mater. Chem. C* **2016**, *4*, 4374–4379. [[CrossRef](#)]
48. Meng, X.F.; Liu, Z.H.; Cui, B.; Qin, D.D.; Geng, H.Y.; Cai, W.; Fu, L.W.; He, J.Q.; Ren, Z.; Sui, J.H. Grain Boundary Engineering for Achieving High Thermoelectric Performance in n-Type Skutterudites. *Adv. Energy Mater.* **2017**, *7*. [[CrossRef](#)]
49. Tang, Y.; Chen, S.-W.; Snyder, G.J. Temperature dependent solubility of Yb in Yb-CoSb_3 skutterudite and its effect on preparation, optimization and lifetime of thermoelectrics. *J. Mater.* **2015**, *1*, 75–84. [[CrossRef](#)]
50. Tang, Y.L.; Hanus, R.; Chen, S.W.; Snyder, G.J. Solubility design leading to high figure of merit in low-cost Ce-CoSb₃ skutterudites. *Nat. Commun.* **2015**, *6*. [[CrossRef](#)] [[PubMed](#)]
51. Rogl, G.; Zhang, L.; Rogl, P.; Grytsiv, A.; Falmbigl, M.; Rajs, D.; Kriegisch, M.; Muller, H.; Bauer, E.; Koppensteiner, J.; et al. Thermal expansion of skutterudites. *J. Appl. Phys.* **2010**, *107*, 043507. [[CrossRef](#)]

